

Multilayered Lipid Membrane Stacks for Biocatalysis Using Membrane Enzymes

George R. Heath, Mengqiu Li, Honling Rong, Valentin Radu, Stefan Frielingsdorf, Oliver Lenz, Julea N. Butt, and Lars J. C. Jeuken*

Multilayered or stacked lipid membranes are a common principle in biology and have various functional advantages compared to single-lipid membranes, such as their ability to spatially organize processes, compartmentalize molecules, and greatly increase surface area and hence membrane protein concentration. Here, a supramolecular assembly of a multilayered lipid membrane system is reported in which poly-L-lysine electrostatically links negatively charged lipid membranes. When suitable membrane enzymes are incorporated, either an ubiquinol oxidase (cytochrome bo_3 from *Escherichia coli*) or an oxygen tolerant hydrogenase (the membrane-bound hydrogenase from *Ralstonia eutropha*), cyclic voltammetry (CV) reveals a linear increase in biocatalytic activity with each additional membrane layer. Electron transfer between the enzymes and the electrode is mediated by the quinone pool that is present in the lipid phase. Using atomic force microscopy, CV, and fluorescence microscopy it is deduced that quinones are able to diffuse between the stacked lipid membrane layers via defect sites where the lipid membranes are interconnected. This assembly is akin to that of interconnected thylakoid membranes or the folded lamella of mitochondria and has significant potential for mimicry in biotechnology applications such as energy production or biosensing.

and chloroplasts. In addition to greater control over compartmentalization, the extra layering of membranes gives the organisms increased area for membrane proteins. The inner membranes of mitochondria, for example, are folded into cristae to greatly increase the surface area available for the electron transport chain proteins, packing high concentrations into a small volume.^[1] Similarly, chloroplasts employ the stacking of interconnected thylakoid membranes to greatly enhance the concentrations of photosynthetic protein complexes required to efficiently harness solar energy.^[2] These structures and many others show how the lamellar stacking of membranes and their proteins hold substantial technological potential for biomimicry, where the stacking of membranes may allow the design of novel protein arrangements with possible applications in catalysis, photonics, sensing, and the 3D crystallization of membrane proteins.^[3,4]

1. Introduction

Double or multilayered membranes, along with their associated membrane proteins, are an integral part of the energy producing pathways of eukaryotic cells, gram-negative bacteria,

Supported lipid bilayers (SLBs) have been widely advocated for biotechnological applications and frequently used as model cell membranes in fundamental studies. SLBs provide a powerful means to study the function of membrane proteins and protein-protein interaction in membranes.^[5-7] The planar nature of SLBs allows investigations by an array of powerful surface analytical techniques such as atomic force microscopy (AFM), quartz crystal microbalance, surface plasmon resonance, and total internal reflection fluorescence microscopy. The potential of SLBs to mimic complex multilayer membrane assemblies has been reported,^[8] yet the development of consistent methodologies has been limited, and only few model systems are described that investigate protein behavior in multiple membranes. For instance, multilamellar membranes are routinely used in studies of the structure of lipid membranes and membrane-associated polypeptides by X-ray or neutron diffraction, or by solid-state nuclear magnetic resonance spectroscopy.^[9] Methodologies used to form these multilayered membranes require the drying of membranes in organic solvents, which is suitable for lipid and peptide studies; however, during drying, membrane proteins are prone to lose their biological activity.^[10]

We have previously reported on a simple layer-by-layer (LBL) methodology to form lipid multilayers via vesicle rupture onto existing SLBs using poly-L-lysine (PLL) as an electrostatic polymer “glue.”^[11] Not only does this technique allow

Dr. G. R. Heath, Dr. M. Li, H. Rong, Dr. V. Radu,
Dr. L. J. C. Jeuken
School of Biomedical Sciences
University of Leeds
Leeds LS2 9JT, UK
E-mail: l.j.c.jeuken@leeds.ac.uk

Dr. S. Frielingsdorf, Dr. O. Lenz
Institut für Chemie, Sekretariat PC14
Technische Universität Berlin
Straße des 17. Juni 135, 10623 Berlin, Germany

Prof. J. N. Butt
Centre for Molecular and Structural Biochemistry
School of Biological Sciences and School of Chemistry
University of East Anglia
Norwich NR4 7TJ, UK

The copyright line of this paper was changed 5 April 2017 after initial publication.

This is an open access article under the terms of the Creative Commons Attribution License, which permits use, distribution and reproduction in any medium, provided the original work is properly cited.

DOI: 10.1002/adfm.201606265



incorporation of membrane proteins, but it can also create membrane stacks with different membrane proteins in each layer. Alternating membrane protein stacks are found in, for example, the electrocyte cells of electric eels in which the trans-membrane proteins are asymmetrically distributed across two primary membranes that, when added in series, can generate potentials of ≈ 600 V.^[12,13]

Here, we engineered a lipid multilayer matrix in which native electron mediators can freely diffuse for bio-electrocatalytic applications. Mimicking the function of cristae and thylakoid stacks in mitochondria and chloroplasts, respectively, the assembly increases the concentration of membrane enzymes per electrode surface area in a stepwise manner. We created multilayers of membrane enzymes in a native-like lipid environment using the LBL assembly of bacterial membrane extracts at gold electrodes. Assemblies with two different membrane proteins are demonstrated: a membrane-bound hydrogenase (MBH) from *Ralstonia eutropha*, which oxidizes H_2 , and a ubiquinol oxidase, cytochrome *bo*₃, from *Escherichia coli* that reduces oxygen. With each deposition of a membrane layer, we see the catalytic activity increasing as the total amount of enzyme on the surface increases. This biomimetic system demonstrates how the stacking of membranes can proportionally increase the concentration of active membrane proteins at surfaces.

2. Results and Discussion

2.1. Interconnected Lipid Multilayers

Initial structural characterization of the membrane stacks was performed on glass and mica using fluorescence microscopy and AFM, respectively. Quinone diffusion between the membrane layers and biocatalytic activity of membrane enzymes incorporated into the stack was then characterized using

electrochemistry, for which the stacks were formed on gold surfaces. The formation of membrane stacks is schematically shown in **Figure 1**.

Figure 2A displays fluorescence images of a single solid supported bilayer membrane (doped with a fluorescent lipid analog) on which a layer of PLL was adsorbed. Before PLL, a homogenous membrane is present as evidenced by a uniform fluorescence intensity across the field of view. After addition of PLL, discrete regions with twofold fluorescent intensity are evident (**Figure 2A,B**). These patches are also seen by AFM (**Figure 2D**), and the height and fluorescence intensity are consistent with the formation of two lipid bilayer membranes on top of each other. These patches appear before adding any additional vesicles. Furthermore, before addition of PLL, no vesicles were detected on top of the base lipid bilayer (**Figure 2A**). This suggests that the lipid required to form the double membrane patches is extracted from the base bilayer. To test if the second “top” membrane patches are continuous with the first membrane beneath, we performed fluorescence recovery after photobleaching (FRAP) experiments (**Figure 2A**). Importantly, after photobleaching both the base lipid membrane and the double membrane patches show full fluorescent recovery with nearly identical rates (**Figure 2B,C**). Analysis of the intensities of the bleached double patches relative to the nonbleached base bilayer (**Figure 2C**) shows recovery to 197% after 20 min. This indicates that fluorescently labeled lipids rapidly diffuse into both membranes in the double membrane patches. Recovery to the double membrane patches can be analyzed in isolation by subtracting fluorescence intensity from the base membrane. Performing this subtraction (**Figure 2C**, black line) results in a fluorescent recovery that is almost indistinguishable from that of the base bilayer (**Figure 2C**, blue line). The lateral diffusion constants of $0.7 \pm 0.2 \mu\text{m}^2 \text{s}^{-1}$ and $0.6 \pm 0.1 \mu\text{m}^2 \text{s}^{-1}$ for the double patches and base bilayer, respectively, indicate that diffusion into double membrane patches is indistinguishable from the lateral diffusion throughout the base bilayer. Such

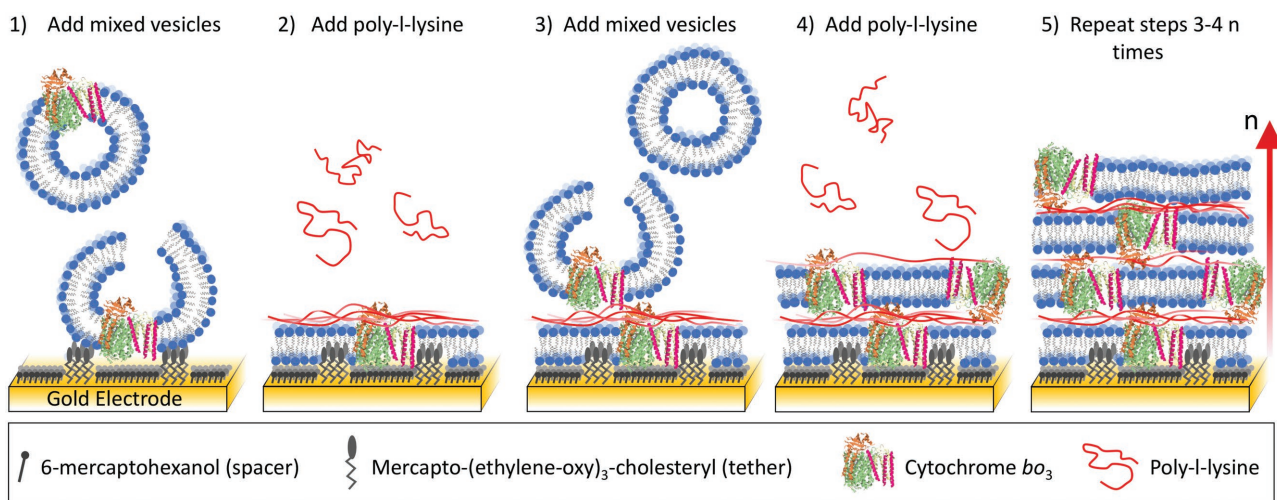


Figure 1. Schematic representation of the method used to create lipid–protein multilayers on gold electrodes. (1) Negatively charged vesicles are added to the gold electrode that has a 6-mercaptohexanol and mercapto-(ethylene-oxy)₃-cholesteryl (at an $\approx 3:2$ ratio) self-assembled monolayer aiding the formation of the first planar lipid bilayer. (2) Poly-L-lysine is bound to the surface of the lipid bilayer creating a net positive surface charge. (3) More negatively charged vesicles are added, which rupture on the poly-L-lysine-coated membrane to form a double membrane. (4) Adsorption of poly-L-lysine to the double membrane. (5) Steps (3) and (4) are repeated *n* times to create *n* additional stacked bilayers.

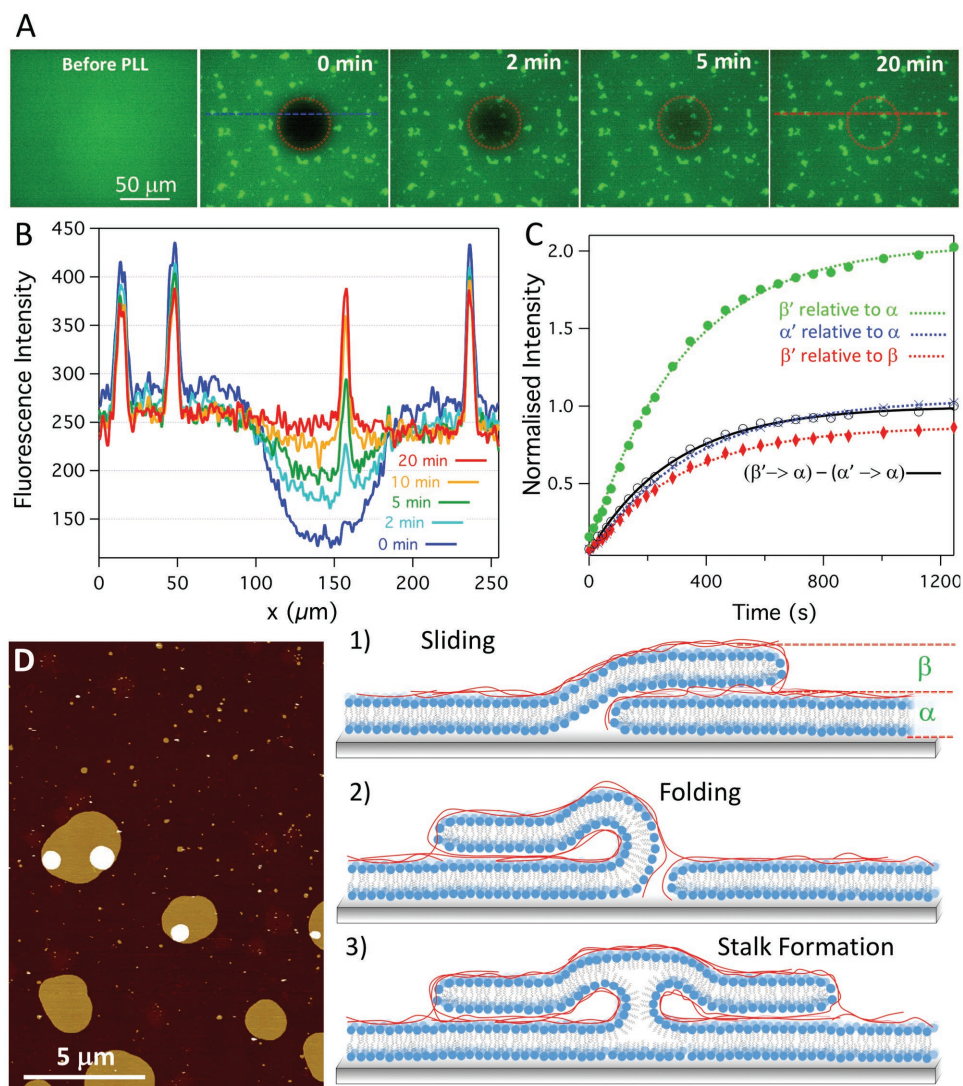


Figure 2. A) Series of fluorescence microscopy images before and after addition of PLL. After addition of PLL, fluorescence recovery is shown after photobleaching a central circular spot of a POPC/POPG 1:1 bilayer (0.5% TxRed DHPE). Note that the patches with double fluorescent intensity are formed only after incubation with PLL. B) Intensity profiles across dashed lines in (A) at different time points. C) Plots of normalized fluorescence intensity change where α and β denote intensity of single and double-bilayer patches, respectively, and prime (α' and β') the intensity within the bleached area. The intensities of the bleached areas are normalized against either the base bilayer (α) or the double membrane patch (β), as indicated. The black line represents the difference between " β' relative to β " and " α' relative to α ", as further explained in the text. D) AFM image of POPC/POPG (1:1) bilayer after incubation with PLL (z-scale = 16.0 nm). The cartoon illustrations show the possible configuration that can allow diffusion between multiple membranes: (1) sliding, (2) folding, or (3) stalk structures. Experiments were performed in 5×10^{-3} M MOPS, pH 7.0, 22 °C.

similar rates of diffusion imply that the two membranes in the double membrane patches are interconnected via a lipid phase. Similar patches of membrane stacks that are connected to an underlying bilayer have previously been observed after the addition of lipopolysaccharide^[14] and, very recently, long chain polyamines.^[15]

As illustrated by the cartoons in Figure 2, there are a number of possible configurations that allow rapid perpendicular diffusion between the base and secondary membranes. Sliding or folding structures may be induced by PLL in regions where the base bilayer had a defect. Alternatively, rapid lipid transfer between vesicles or from vesicles to a supported lipid bilayer has previously been reported when the lipids adopt a so-called

stalk structure.^[16,17] Typically, these stalks, which may be stabilized by PLL, require two proximal leaflets to form a local neck-like connection, resulting in a rapid lipid exchange between the opposing membranes through lipid diffusion in the connected leaflets.^[18]

The formation of double membrane patches was monitored in situ by AFM, which showed, upon addition of PLL, the immediate formation (within tens of seconds; see Figure S1 in the Supporting Information) of double membrane patches with clearly distinct sizes (Figure 2D): those with large diameters of 500–5000 nm (3% by number) and those with diameters averaging 90 ± 40 nm (the remaining 97%). The size of the smaller patches remained stable over time, but larger patches

were observed to grow across the bilayer asymmetrically (i.e., in one direction only; see Figure S1 in the Supporting Information). Although the resolution of the AFM is not sufficient to confirm this, we speculate that the larger patches are created by sliding or folding of the membrane, consistent with the growth in one direction only, and the smaller patches are due to the stalk formation.

The further addition of negatively charged vesicles to bilayers coated with PLL produces an almost complete second bilayer. AFM indicates that the new second lipid bilayer membrane seamlessly connects to the previous double membrane patches (Figure S2, Supporting Information). It is thus possible that the structures shown schematically in Figure 2 are maintained when multilayers are formed. Further addition of PLL to this double membrane produces an even higher density of third bilayer patches, while closing up the second bilayer. This process continues with each additional bilayer, potentially providing diffusion routes between the whole multilayer.

2.2. Quinone Diffusion in Lipid Multilayers

Quinones are typical coenzymes in electron transport chains and shuttle electrons between many membrane proteins that are associated with energy conservation/transduction. The FRAP experiments described above suggest that lipids rapidly diffuse between lipid membranes in the multilayer membrane patches. It is therefore likely that lipophilic quinones such as ubiquinone-10 (UQ10) and menaquinone-7 (MQ7), which stay in the hydrophobic region of the bilayer, should also transfer between membranes. To test this hypothesis and to confirm the presence of intermembrane connections, quinone-mediated electron transfer across stacked lipid membranes was investigated by cyclic voltammetry of lipid multilayers containing MQ7 or UQ10. The multilayers were built up layer-by-layer on mixed self-assembled monolayers (SAMs) on the surface of gold electrodes. To adhere the first “base” lipid layer, the membrane was tethered to the surface with previously established methods.^[19,20] In short, a mixed SAM was formed on a gold electrode composed of mercapto-(ethylene-oxy)₃-cholesteryl (membrane tether, EO3C) and 6-mercaptohexanol (spacer). The “base” lipid membrane was then formed via self-assembly from lipid vesicles, where the cholesterol tether induces rupture of the vesicle and allows the formation of a continuous planar lipid membrane (the “base” lipid membrane). Consecutive membrane layers were then formed by alternatively adsorbing PLL and vesicles (Figure 1). **Figure 3A** shows a series of cyclic voltammograms (CVs) of the SAM only, a 1:1 (w/w) POPC/POPG base membrane containing 1.5% (w/w) MQ7 and then each response after four cycles of incubation with PLL followed by 3:1 POPC/POPG 1.5% (w/w) MQ7 vesicles. These lipid compositions were chosen since we have previously shown that this protocol creates additional membranes with each PLL/vesicle incubation cycle on mica, glass, and SiO₂.^[11] The CV of the first bilayer shows the MQ7 reduction (≈ -0.45 V vs standard hydrogen electrode, SHE) followed by oxidation (≈ 0.1 V vs SHE) peaks. The large peak separation is partly caused by the thickness of the 6-mercaptohexanol layer in the SAM, reducing the electronic coupling

between electrode and MQ7. More importantly, however, it is caused by the coupling of the electron transfer with protonation/deprotonation steps, which are slow due to the lipid bilayer environment.^[21] With each additional bilayer we observe a linear increase in the current being transferred by the MQ7 (i.e., increase in peak area), implying an increase in the number of quinones that electrochemically interact with the electrode.

The double-layer capacitance of the multilayer stacks was estimated by electrochemical impedance spectroscopy (Figure 3B). The formation of the first bilayer produced a double-layer capacitance of $\approx 1.2 \pm 0.1 \mu\text{F cm}^{-2}$ as estimated from the diameter in the Cole–Cole plot. The capacitance is in agreement with previous similar lipid membranes on the EO3C system.^[22] However, with each additional bilayer we observe only small reductions in the double-layer capacitance, indicating that the additional lipid bilayers have low resistance to ions and thus likely contain defects.

CV analysis of the total charge transferred by MQ7 (Figure 3C) shows a linear increase for each additional lipid membrane in the multilayer stack. An identically formed multilayer stack with UQ10 showed the same behavior (Figure S3, Supporting Information). To determine if electron transfer was limited by diffusion, CVs were performed on an eight-layered system with scan rates varying between 10 and 200 mV s⁻¹ (Figure 3D). The redox peak area shows no dependency on scan rate, indicating that up to 200 mV s⁻¹, UQ10 diffusion is not limiting. There are no analytical solutions available to calculate the diffusion in complex multilayered film systems such as these, but it is clear that even in an eight-layered membrane system, UQ10 in all layers is oxidized or reduced in less than a second.

Although synthetic lipids offer a stable environment for membrane proteins, activity of membrane proteins can be dependent on the presence of particular annular lipids.^[23] For bacterial membrane enzymes, it can thus be beneficial to provide a more native lipid environment via the use of bacterial lipid extracts. To study the layer-by-layer formation of multilayers composed of lipid extracts, we used *E. coli* “polar” lipid extracts, which according to the supplier contain $\approx 23\%$ phosphoglycerol (PG), 10% cardiolipin, and 67% phosphoethanolamine (w/w). The PG and cardiolipins give these membranes an overall negative charge, as required for our LBL system with the positively charged PLL. Figure 3E shows CVs at each stage after incubating five cycles of *E. coli* polar extract vesicles containing 1% (w/w) UQ10. As with the POPC/POPG system, we observe an increase in the quinone redox peaks with each addition of vesicles/PLL. This suggests that, as long as the lipid mixture contains sufficient negative charge, the LBL system can be adapted to any lipid composition. It should be noted that *E. coli* polar extract lipid also contains small amounts of ubiquinone-8, native to *E. coli*.

From our results, the transfer of charge across multiple membranes to the electrode via the reduction and oxidation of the quinones is clear. What remains unclear is the mechanism of how this process occurs. While AFM and fluorescence results suggest there are connections between adjacent bilayers, allowing diffusion perpendicular to the plane of the lipid membranes, there may be a number of other possible

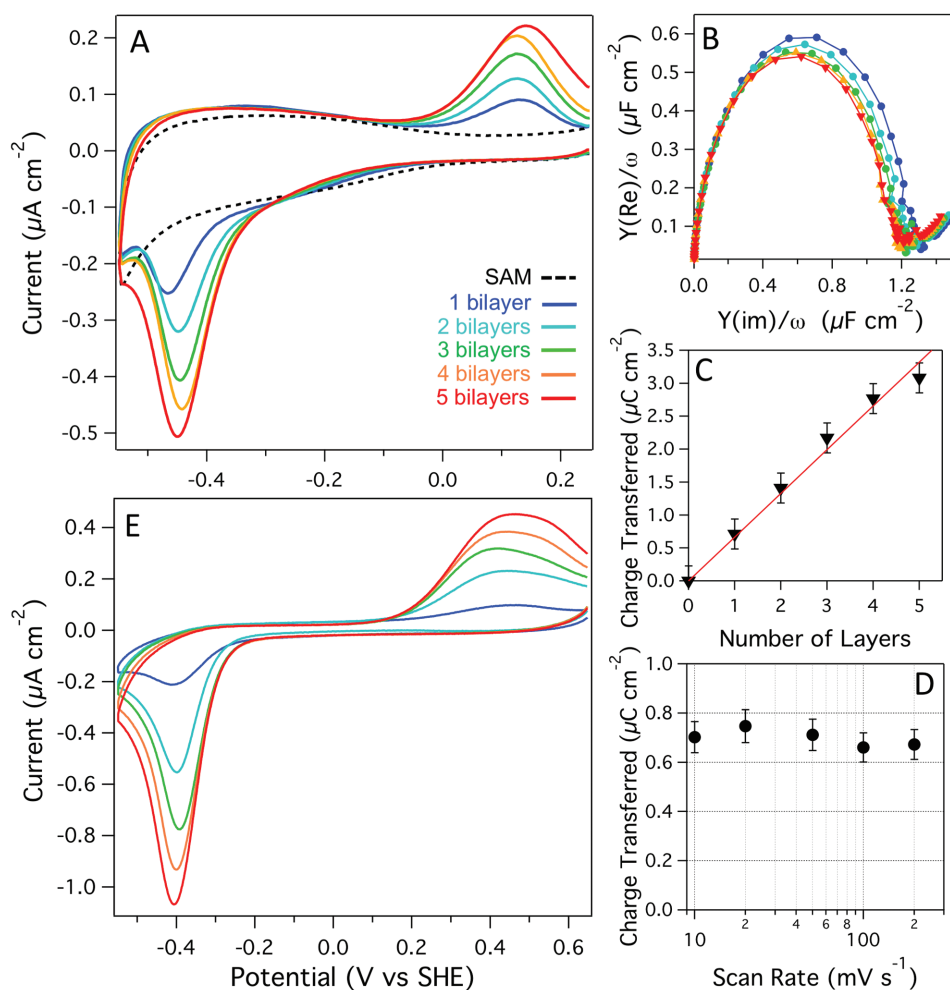


Figure 3. A) Cyclic voltammograms, B) Cole–Cole plots, and C) total charge transferred during MQ7 reduction of POPC-POPG (1.5% MQ7)/PLL multilayers. D) Charge transferred (reduction of UQ10) in CVs as a function of scan rate for a POPC-POPG (0.5% UQ10)/PLL multilayer with eight layers. E) Cyclic voltammograms of *E. coli* polar lipid (1% UQ10)/PLL multilayers (color coding as in (A)). Experiments were performed in the absence of O_2 and at 10 mV s^{-1} scan rates, $20 \times 10^{-3} \text{ M}$ MOPS, $30 \times 10^{-3} \text{ M}$ Na_2SO_4 , pH 7.4, 20°C .

transfer routes such as quinone–quinone electron transfer, where a quinone in one bilayer passes an electron to a quinone in the adjacent bilayer, or quinone hopping across membranes. To further test the mechanism of electron transport, a double membrane system was prepared in which the quinones were omitted in the base bilayer. In the latter system, the reduction and oxidation of the quinones is still observed (Figure S4, Supporting Information) confirming that the quinones are able to diffuse between the membranes layers. Spontaneous lipid transfer between membranes is very slow (timescale of hours).^[24,25] To test if the same applies to UQ10 transfer, a single-membrane layer was formed without UQ10 and incubated with a liposome solution containing UQ10. As expected, no UQ10 was observed to transfer from the liposomes in solution to the membrane on the surface (Figure S5, Supporting Information). Finally, to exclude direct quinol to quinone electron transfer across membranes, single bilayers containing UQ10 were formed and incubated with liposomes also containing UQ10. The addition of liposomes did not alter the UQ10 signals, confirming that electrons are not passed on

from the membrane on the surface to liposomes in solution (Figure S5, Supporting Information). Taken together, these results strongly suggest that the primary mechanism is diffusion of quinols through the lipid interconnections between the membrane stacks.

For a given molecule to transfer between two adjacent membranes, it needs to diffuse a certain distance to the nearest membrane connection. As determined from AFM images of double membrane patches on the base bilayer, the average nearest neighbor distance between patches is 470 nm ($\text{SD} \pm 250 \text{ nm}$). Assuming a quinone or lipid molecule would need to travel on average half this distance to reach an inter-membrane connection, we can roughly estimate the time taken (t) to diffuse this distance (x) using the 2D diffusion equation: $t = x^2/4D$, where D is the diffusion constant. Given the lateral diffusion constant of $2 \mu\text{m}^2 \text{ s}^{-1}$ for UQ10^[26] it would take $\approx 0.01 \text{ s}$ to diffuse to the next bilayer in the multilayer. This timescale corresponds to the fact that it takes less than a second to oxidize or reduce all UQ10 in an eight-layered membrane system (see above).

2.3. Cytochrome *b*₀₃ Lipid Multilayers

The rapid distribution of electrons via quinones across the multilayer assembly should allow the electrochemical control of membrane-bound quinone oxidoreductases incorporated in such an array. As a proof of principle, the ubiquinol oxidase from *E. coli*, cytochrome *b*₀₃ (cyt *b*₀₃) was studied. As part of the aerobic respiratory pathway, cyt *b*₀₃ catalyzes the oxidation of ubiquinol to ubiquinone (UQ10) and reduces molecular oxygen to water (Figure 4A).^[27] *E. coli* membrane

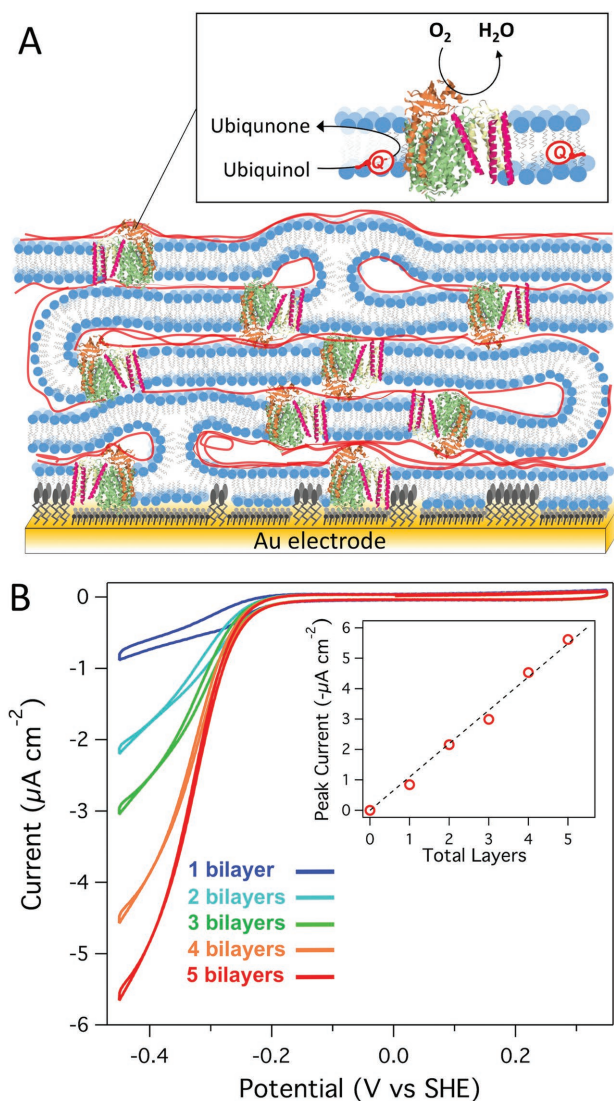


Figure 4. A) Illustration of the possible interconnected multilayer membrane structure containing cyt *b*₀₃. The ubiquinone is reduced at the electrode to ubiquinol, which is then reoxidized by cyt *b*₀₃, catalyzing the reduction of oxygen to water. B) CVs of one to five bilayer stacks containing cyt. *b*₀₃ prepared by mixed liposomes (2:8 mixture of cytoplasmic membrane extract of *E. coli* producing cyt *b*₀₃ and *E. coli* “polar” lipid extract). Inset: Catalytic current measured at -450 mV versus SHE as a function of the number of bilayers. Measurements were made in air saturated buffer solution ($\approx 250 \times 10^{-6}$ M oxygen) without stirring/rotation, at a scan rate of 10 mV s^{-1} and in 20×10^{-3} M MOPS, 30×10^{-3} M Na_2SO_4 , pH 7.4, 20 °C.

extracts containing overproduced cyt *b*₀₃ were mixed with *E. coli* “polar” lipid extracts (supplemented with 1% UQ10 (w/w)) at 2:8 protein mass to *E. coli* lipids mass ratio. Freeze-thaw cycles and 200 nm extrusion were used to mix membrane extracts and liposomes. Addition of these vesicles to the gold electrodes modified with the cholesterol tether, EO3C, produced a double-layer capacitance of $0.82 \mu F cm^{-2}$ confirming the formation of a tethered lipid bilayer.^[28] Figure 4B shows the catalytic activity as measured by CV of the cyt *b*₀₃ for the base bilayer and four subsequent bilayers formed via repeated cycles of PLL and cyt *b*₀₃/*E. coli* mixed vesicles (in the presence of surplus oxygen). At low electrode potentials (<0.2 V) quinone is reduced to quinol at the electrode and diffuses to cyt *b*₀₃ where it is oxidized by the enzyme, coupled to the reduction of oxygen. If only one bilayer is prepared, the catalytic wave is in close agreement with our previous reported studies of cyt *b*₀₃ with a catalytic current of $0.84 \pm 0.05 \mu A cm^{-2}$.^[28,29] After absorption of PLL followed by the formation of a second cyt *b*₀₃-containing membrane, we observe a 2.5-fold increase in the catalytic current. With each additional membrane formation, we observed further increases in the current. Plotting the catalytic current at -0.45 V (Figure 4B, inset) gives a linear increase against the number of bilayers, indicating cyt *b*₀₃ is accessed by ubiquinol molecules in all layers and the catalytic current is not limited by O_2 or quinone diffusion through the membranes (i.e., catalysis is limited by the amount of cyt. *b*₀₃ in the total membrane stack). From the catalytic current and the surface coverage of UQ10, the turnover rate of UQ10 can be estimated. The catalytic current of a five-membrane system is $5.5 \mu A cm^{-2}$ (Figure 4B, 1% (w/w) UQ10 in *E. coli* polar lipid extracts). The total charge of UQ10 in a five-membrane system is $\approx 10 \mu C cm^{-2}$ (1% (w/w) UQ10 in *E. coli* polar lipid extracts; Figure 3E), and thus, on average, UQ10 receives an electron every $(10 \mu C cm^{-2} \div 5.5 \mu A cm^{-2}) \approx 1.8$ s. Taking into account that UQ10 reduction is a two-electron reaction, UQ10 is on average reduced by the electrode every 3.6 s and thus the estimated diffusion to the next membrane is order of magnitude faster (≈ 0.01 s; see above).

2.4. Hydrogenase Lipid Multilayers

Membrane-bound hydrogenases (uptake hydrogenases) are a class of enzymes that catalyze the reversible oxidation of H_2 to protons via the reduction of quinones (Figure 5A).^[30] The rates at which hydrogenases interconvert H_2 to H^+ is comparable to those normally achieved by Pt making them potential catalysts for H_2/O_2 biofuel cells.^[31] In this study we have used an O_2 -tolerant [NiFe]-hydrogenase, the MBH from the β -proteobacterium *R. eutropha*, capable of maintaining a high level of activity in the presence of air supplemented with low H_2 concentrations.^[32–34] Similar to many other uptake [NiFe]-hydrogenases, its structure consists of three subunits, one of which is an integral membrane protein (Figure 5A).^[35,36]

Forming a single bilayer from MBH membrane extracts (mixed with *E. coli* lipids) on the cholesterol-mixed SAM produced similar results to previous reports with the same MBH/membrane system.^[33] CVs recorded under 100% N_2 show no catalytic oxidation waves, while in the presence of 5% H_2 , the onset of H_2 oxidation coincides with ubiquinol oxidation

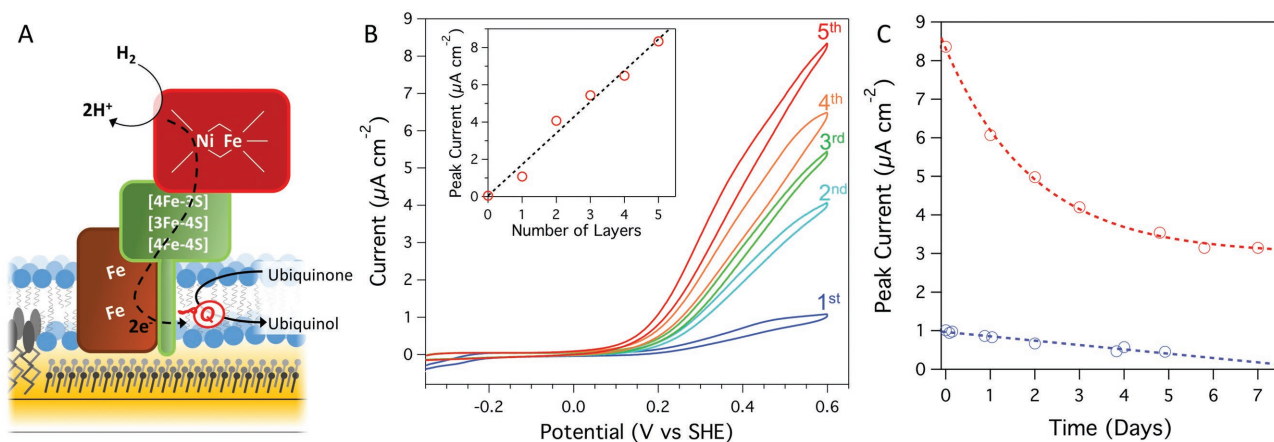


Figure 5. A) Illustration of MBH activity on the membrane-modified electrodes. Ubiquinone is reduced by the cytochrome b_{562} subunit (brown) to ubiquinol using electrons generated from hydrogen oxidation. The ubiquinone is reoxidized at the electrode. B) CVs for one to five bilayers containing MBH prepared by mixed liposomes (4:10 mixture of cytoplasmic membrane extract of *R. eutropha* expressing MBH and *E. coli* “polar” lipid extract). Inset: Catalytic current (measured at 600 mV) as a function of the number of bilayers. C) Peak current (obtained at 600 mV) as a function of time (up to a week) for a five-layered MBH multilayer (red) and a single-MBH bilayer (blue) as measured by CV. In between measurements, the electrochemical cell was stored at 30 °C under nitrogen in the absence of an applied potential. Measurements were made in 5% hydrogen, 95% nitrogen buffer solution without stirring at a scan rate of 10 mV s⁻¹ in 20 × 10⁻³ M MOPS, 30 × 10⁻³ M Na₂SO₄, pH 7.4, at 30 °C.

(Figure 5B; compare to Figure 3E), confirming that the electron transfer between the MBH and the electrode is mediated by the quinone pool. With each additional bilayer, we observed an increase in the catalytic current, indicating additional hydrogenase is added with each membrane layer that is formed (Figure 5B, inset). Due to the presence of the cholesterol tethers we note that the first membrane is expected to have slightly less enzyme and thus less catalytic activity, compared to the second and subsequent membranes.

These studies show that our layer-by-layer methodology is able to multiply activity for both quinone oxidizing and quinone reducing membrane proteins. Previous studies of multilayers with water soluble, globular, enzymes report that the Faradaic current from the protein increases linearly with the number of layers; however, this can saturate after as few as three layers.^[37–39] This saturation has been attributed to a limited diffusion of the enzyme’s substrate through the increasingly thick multilayer and/or limited electron transfer rates to the electrode. We do not observe such limitations in our studies for up to 5 interconnected lipid membranes. However, we anticipate that the number of beneficial layers will ultimately be limited by the diffusion rate of the quinones, which we have shown to be very fast, and the diffusivity of substrate through the membranes. The diffusion rate of quinones or other electron mediators across layers in the multilayer could be increased by creating a system with more lipid connections. We would expect the inclusion of lipids with a greater preference for lipid curvature may allow this. Alternatively, non-native lipophilic electron mediators could be used (instead of the native substrates MQ7/UQ10), which may have faster diffusion rates and preferable redox potentials.^[40]

Hydrogenases have been advocated as hydrogen-oxidizing biocatalysts in hydrogen–oxygen fuel cells.^[32,41–46] To perform such function, both the biocatalyst and the electrochemical system require a high stability and endurance. We thus tested the stability of the MBH multilayers by performing CV scans at

intervals over several days while keeping the sample at 30 °C. The results (Figure 5C) show an initial sharp 25% decrease in activity over the first 24 h, which decays to a plateau at 40% after 5 d. The stability of a system with only a single MBH bilayer shows a linear drop in activity with no plateau. This suggests that the multilayer stack could be a better environment for the protein. In comparison, previous protein film studies by Reisner et al. have shown that the activity of globular hydrogenases immobilized on graphite electrode surfaces can exhibit losses as high as 50% in the first hour and 90% after 1 d. However, the stability of the hydrogenase was found to be greatly increased on TiO₂–indium tin oxide (ITO) electrodes where 80% of the electrocatalytic activity was retained after 48 h and 50% after one month storage in an electrolyte solution.^[47] Additionally, redox active hydrogels have been shown to significantly improve hydrogenase stability, allowing constant turnover for over 2 weeks with only slight decrease in activity.^[48] Carbon electrodes with hydrogenase immobilized by covalent bonds have also been found to be very stable. After an initial ≈30% loss of the catalytic current during the first 2 d, there was very little decrease after a month of continuous operation.^[49]

3. Conclusions

Our study shows how a simple layer-by-layer method can be used to create biomimetic interconnected lipid multilayers, which allow the concentration of redox-active membrane enzymes at surfaces to be multiplied. The ability to incorporate a high density of active membrane enzymes using mixed membrane extracts highlights the system’s adaptability (as long as there is sufficient negatively charged lipid). Two membrane-bound quinone-converting enzymes were used to demonstrate the application of these assemblies as bio-electrocatalytic systems, using UQ10 as electron mediator. The interconnections between the membrane layers proved vital in the ability of

UQ10 to diffuse through the multilayered membrane system. By changing the enzymes and electron mediators used, this biomimetic system has potential for many other applications such as biosensors with greater sensitivity or photovoltaic cells with greater power output. By varying pH, PLL length, polyelectrolyte, or lipid composition, it may be possible to control both the interconnections and spacing between membranes. Such control over the 3D self-assembly would allow a range of assemblies to be constructed to directly model the protein interactions or lipid configurations in biological double and multilayered systems such as mitochondria and thylakoids.

4. Experimental Section

Materials: Template stripped gold (TSG) surfaces and SAMs were prepared as previously described.^[22,28] SAMs were obtained by incubating TSG surfaces in isopropanol containing different ratios of mercapto-(ethylene-oxy)3-cholesteryl (membrane tether, EO3C) to 6-mercaptohexan-1-ol (6MH) to give a total of 1×10^{-3} M thiol compounds (≈ 16 h).^[22] The slides were rinsed with propanol and methanol and dried under nitrogen before being incorporated into the electrochemical cell. If not otherwise stated, all chemicals were purchased from Sigma-Aldrich (Dorset, UK). 1,2-palmitoyl-2-oleoyl-*sn*-glycero-3-phosphocholine (POPC), palmitoyl-2-oleoyl-*sn*-glycero-3-phosphoglycerol (POPG), and *E. coli* polar lipid extract were obtained from Avanti Polar Lipids (Alabaster, AL). Texas Red 1,2-dihexadecanoyl-*sn*-glycero-3-phosphoethanolamine (TxRed DHPE) was purchased from Molecular Probes. Ultrapure water (resistance 18.2 M Ω cm) from a Milli-Q system was used throughout.

Vesicle Preparation: Dried lipid–quinone mixtures were hydrated in 5×10^{-3} M 3-(N-Mmorpholino)propanesulfonic acid (MOPS) at pH 7.0 to 5 mg mL⁻¹ and extruded through a 200 nm track etched membrane (11 times). For experiments without membrane enzymes, these vesicles were used to form lipid bilayers as described below. For experiments with membrane enzymes, mixed vesicles were formed. The extruded liposomes were mixed with cytoplasmic membrane extracts (either from *E. coli* or *R. eutropha*) to obtain a ratio of dry lipids to dry total protein (as determined by bicinchoninic acid (BCA) assays) of 10:4 (for the MBH experiments) and 8:2 (for cytochrome *bo*₃ experiments). The obtained mixture was subjected to three freeze-thaw cycles and then extruded again through 200 nm 11 times. The preparation of the cytoplasmic membrane extracts is described below.

Lipid Multilayer Formation on Gold Electrodes: Lipid multilayers on TSG electrodes were formed layer-by-layer using vesicle rupture, first onto an EO3C/6MH SAM and then by alternating layers PLL and vesicles. To form the base tethered bilayer on TSG electrode with a mixed EO3C/6MH SAM (with a surface coverage of EO3C between 30% and 50%) the vesicle solution was added at 0.5 mg mL⁻¹ with 5×10^{-3} M CaCl₂ at room temperature for 1 h. The bilayer was rinsed five times with deionized water, five times with 1×10^{-3} M ethylenediaminetetraacetic acid (EDTA) followed by at least 15 washes with 5×10^{-3} M MOPS buffer at pH 7.0. PLL (70–150 kDa) was then added to the base bilayer at 10 μ g mL⁻¹ in the same buffer and incubated for 45 min, followed by rinsing 20 times with buffer. To form the second bilayer, the vesicle solution was added at 0.5 mg mL⁻¹ (without CaCl₂) and left to incubate for 1 h followed by rinsing 20 times with buffer. To form additional bilayers, the steps to form the second bilayer were repeated, i.e., incubating PLL, followed by rinsing then incubating vesicle solution.

Lipid Multilayer Formation on Glass Coverslips and Mica: AFM and FRAP experiments were performed with mica and glass coverslips, respectively. For these two substrates, the first base lipid bilayer was formed by incubating the substrates with POPC/POPG (1:1) vesicle solution at 0.5 mg mL⁻¹ with 5×10^{-3} M CaCl₂ at room temperature for 30 min. The bilayer was rinsed five times with 1×10^{-3} M (EDTA followed by at least 15 washes with 5×10^{-3} M MOPS buffer at pH7.0.

Cytochrome *bo*₃ Cytoplasmic Membrane Extraction: *E. coli* cytoplasmic membranes were prepared as previously described^[29] from strain GO105/pJRhIsA in which the cytochrome *bo*₃ protein is overexpressed. *E. coli* was grown to mid-log phase at 37 °C with shaking in LB (Lysogeny Broth) medium supplemented with 5×10^{-4} M CuSO₄ and 100 μ g mL⁻¹ carbenicillin. *E. coli* cells were harvested from the growth medium by centrifugation at 12 000 g for 30 min and the cell paste was frozen at –20 °C overnight. Thawed *E. coli* cell paste was resuspended in MOPS/Na₂SO₄ buffer at ≈ 30 mL of buffer per 10 g of cell paste and passed through a cell disrupter (Constant Systems) at 30 kPsi. Cell debris was removed by centrifugation at 12 000 g for 30 min. The supernatant containing the membrane fraction was centrifuged at 41 000 rpm (Ti45 rotor, Beckman) for 2 h and the membrane pellet was resuspended in 25% (w/w) sucrose-MOPS/Na₂SO₄ buffer. A 30% (w/w) to 55% (w/w) sucrose gradient with centrifugation at 41 000 rpm (Ti45 rotor, Beckman) for 16 h with no deceleration or breaking was used to separate the cytoplasmic membrane from the outer membrane. The cytoplasmic membrane fraction was removed from the sucrose gradient and diluted several times with buffer and centrifugation at 41 000 rpm (Ti45 rotor, Beckman) for 2 h. The protein concentration of the cytoplasmic membrane preparation was determined using a BCA assay. Cytoplasmic membrane vesicles were resuspended in buffer and stored at –80 °C.

Membrane-Bound Hydrogenase Cytoplasmic Membrane Extraction: Media and growth conditions for *R. eutropha* H16 have been previously described elsewhere.^[50] Cytoplasmic membranes were prepared from total membranes of *R. eutropha* HF632 (MBH expression strain) by sucrose gradient centrifugation, as described for the cytochrome *bo*₃ *E. coli* cytoplasmic membrane extraction.

Cyclic Voltammetry and Electrochemical Impedance Spectroscopy: Electrochemical measurements were carried out in a three-electrode configuration electrochemical cell described previously, using either a silver–silver chloride or mercury–mercury sulfate reference electrode.^[28] All potentials are quoted versus the SHE ($E_{\text{SHE}} = E_{\text{Hg}/\text{Hg}_2\text{SO}_4} + 651$ mV at 25 °C; $E_{\text{SHE}} = E_{\text{Ag}/\text{AgCl}} + 199$ mV at 25 °C). A Pt wire was used as the counter electrode. The electrochemical cell was housed in a Faraday cage (for electrical noise minimization). Experiments with MBH were performed inside a nitrogen-filled glove box (MBraun Lab Master sp), which maintains oxygen levels below 0.1 ppm. Gases were bubbled into the cell solution at constant flow rates using gas mass flow controllers (Smart-Trak Series 100, Sierra Instruments, accuracy: 1% of full range). The gases used were nitrogen (oxygen-free, BOC) and a 95% nitrogen-5% hydrogen mixture (BOC). Electrochemical measurements were carried out using an Autolab (Eco-chemie) electrochemical analyzer equipped with a PGSTAT30 potentiostat, SCANGEN module and an FRA2 frequency analyzer. All electrochemical measurements were performed in 20×10^{-3} M MOPS, 30×10^{-3} M Na₂SO₄, pH 7.4.

Atomic Force Microscopy: AFM experiments were performed at room temperature (22 °C) in aqueous conditions using a Dimension FastScan Bio (Bruker). Oxide sharpened silicon nitride tips (Bruker) with typical spring constants of 0.7 N m⁻¹ were used in either PeakForce tapping mode or tapping mode. All images were performed on mica substrates mounted on Teflon discs.

Fluorescence/FRAP: FRAP data were recorded using an epifluorescence microscope (Nikon ECLIPSE Ti). The sample was illuminated and bleached using a high-pressure mercury arc lamp. The bleached spot had a diameter of 55 μ m viewed using a $\times 40$ objective lens. After bleaching, a series of time-lapse fluorescence images were collected using a Zyla sCMOS 5.5 CCD camera (Andor Technology Ltd. Belfast, UK) with the aid of NIS elements software (Nikon, USA). The Axelrod method was employed to calculate the diffusion coefficient and the mobile fraction of the supported lipid bilayer.^[51,52]

Supporting Information

Supporting Information is available from the Wiley Online Library or from the author.

ACKNOWLEDGEMENTS

The research leading to these results received funding from the BBSRC (BB/L020130/1 and BB/L022176/1), the European Research Council under the European Union's Seventh Framework Programme (FP/2007-2013)/ERC Grant Agreement No. 280518, and the German Research Foundation (DFG) via the Cluster of Excellence "Unifying Concepts in Catalysis."

Received: November 28, 2016

Revised: February 13, 2017

Published online: March 21, 2017

- [1] F. Fontanesi, *Mitochondria: Structure and Role in Respiration*, Wiley, Chichester, UK **2001**.
- [2] K. Keegstra, K. Cline, *Plant Cell* **1999**, *11*, 557.
- [3] L. Tayebi, Y. Ma, D. Vashae, G. Chen, S. K. Sinha, A. N. Parikh, *Nat. Mater.* **2012**, *11*, 1.
- [4] B. Bechinger, *Nat. Mater.* **2012**, *11*, 1005.
- [5] M. Khan, N. Dosoky, J. Williams, *Int. J. Mol. Sci.* **2013**, *14*, 21561.
- [6] M. Tanaka, E. Sackmann, *Nature* **2005**, *437*, 656.
- [7] E. Sackmann, *Science* **1996**, *271*, 43.
- [8] J. Xu, D. A. Lavan, *Nat. Nanotechnol.* **2008**, *3*, 666.
- [9] B. Bechinger, J. M. Resende, C. Aisenbrey, *Biophys. Chem.* **2011**, *153*, 115.
- [10] J. H. Crowe, L. M. Crowe, J. F. Carpenter, A. S. Rudolph, C. A. Wistrom, B. J. Spargo, T. J. Anchordoguy, *Biochim. Biophys. Acta, Rev. Biomembr.* **1988**, *947*, 367.
- [11] G. R. Heath, M. Li, I. L. Polignano, J. L. Richens, G. Catucci, P. O'Shea, S. J. Sadeghi, G. Gilardi, J. N. Butt, L. J. C. Jeuken, *Biomacromolecules* **2016**, *17*, 324.
- [12] M. Altamirano, *J. Cell. Comp. Physiol.* **1955**, *46*, 249.
- [13] C. D. Hopkins, *Encyclopedia of Neuroscience*, 3, Academic Press, Oxford **2009**.
- [14] P. G. Adams, L. Lamoureux, K. L. Swingle, H. Mukundan, G. A. Montaño, *Biophys. J.* **2014**, *106*, 2395.
- [15] O. Gräß, M. Abacilar, F. Daus, A. Geyer, C. Steinem, *Langmuir* **2016**, *32*, 10144.
- [16] G. Lei, R. C. MacDonald, *Biophys. J.* **2003**, *85*, 1585.
- [17] V. Knecht, S.-J. Marrink, *Biophys. J.* **2007**, *92*, 4254.
- [18] S. R. Tabaei, J. J. Gillissen, S. Vafaei, J. T. Groves, N.-J. Cho, *Nanoscale* **2016**, *8*, 13513.
- [19] L. J. C. Jeuken, S. D. Connell, P. J. F. Henderson, R. B. Gennis, S. D. Evans, R. J. Bushby, *J. Am. Chem. Soc.* **2006**, *128*, 1711.
- [20] L. M. Williams, S. D. Evans, T. M. Flynn, A. Marsh, P. F. Knowles, R. J. Bushby, N. Boden, *Langmuir* **1997**, *13*, 751.
- [21] G. J. Gordillo, D. J. Schiffrin, *Faraday Discuss.* **2000**, *116*, 89.
- [22] L. J. C. Jeuken, N. N. Daskalakis, X. Han, K. Sheikh, A. Erbe, R. J. Bushby, S. D. Evans, *Sens. Actuators, B* **2007**, *124*, 501.
- [23] C. Hunte, S. Richers, *Curr. Opin. Struct. Biol.* **2008**, *18*, 406.
- [24] L. R. McLean, M. C. Phillips, *Biochemistry* **1981**, *20*, 2893.
- [25] J. W. Nichols, R. E. Pagano, *Biochemistry* **1981**, *20*, 2783.
- [26] D. Marchal, W. Boireau, J. M. Laval, J. Moiroux, C. Bourdillon, *Biophys. J.* **1998**, *74*, 1937.
- [27] J. A. García-Horsman, B. Barquera, J. Rumbley, *J. Bacteriol.* **1994**, *176*, 5587.
- [28] S. A. Weiss, R. J. Bushby, S. D. Evans, P. J. F. Henderson, L. J. C. Jeuken, *Biochem. J.* **2009**, *417*, 555.
- [29] S. A. Weiss, R. J. Bushby, S. D. Evans, L. J. C. Jeuken, *Biochim. Biophys. Acta* **2010**, *1797*, 1917.
- [30] J. Fritsch, O. Lenz, B. Friedrich, *Nat. Rev. Microbiol.* **2013**, *11*, 106.
- [31] A. K. Jones, E. Sillery, S. P. J. Albracht, F. A. Armstrong, *Chem. Commun.* **2002**, *8*, 866.
- [32] J. A. Cracknell, A. F. Wait, O. Lenz, B. Friedrich, F. A. Armstrong, *Proc. Natl. Acad. Sci. USA* **2009**, *106*, 20681.
- [33] V. Radu, S. Frielingsdorf, S. D. Evans, O. Lenz, L. J. C. Jeuken, *J. Am. Chem. Soc.* **2014**, *136*, 8512.
- [34] V. Radu, S. Frielingsdorf, O. Lenz, L. J. C. Jeuken, *Chem. Commun.* **2016**, *52*, 2632.
- [35] J. Fritsch, P. Scheerer, S. Frielingsdorf, S. Kroschinsky, B. Friedrich, O. Lenz, C. M. T. Spahn, *Nature* **2011**, *479*, 249.
- [36] S. Frielingsdorf, T. Schubert, A. Pohlmann, O. Lenz, B. Friedrich, *Biochemistry* **2011**, *50*, 10836.
- [37] M. K. Beissenhirtz, F. W. Scheller, F. Lisdat, *Anal. Chem.* **2004**, *76*, 4665.
- [38] O. Yehzekeli, R. Tel Vered, D. Michaeli, R. Nechushtai, I. Willner, *Small* **2013**, *9*, 2970.
- [39] K. R. Stieger, D. Ciornii, A. Kölsch, M. Hejazi, H. Lokstein, S. C. Feifel, A. Zouni, F. Lisdat, *Nanoscale* **2016**, *8*, 10695.
- [40] F. J. Rawson, A. J. Downard, K. H. Baronian, *Sci. Rep.* **2014**, *4*, 5216.
- [41] S. Krishnan, F. A. Armstrong, *Chem. Sci.* **2012**, *3*, 1015.
- [42] A. F. Wait, A. Parkin, G. M. Morley, L. dos Santos, F. A. Armstrong, *J. Phys. Chem. C* **2010**, *114*, 12003.
- [43] K. Monsalve, I. Mazurenko, C. Gutierrez-Sanchez, M. Ilbert, P. Infossi, S. Frielingsdorf, M. T. Giudici-Ortoni, O. Lenz, E. Lojou, *ChemElectroChem* **2016**, *3*, 2179.
- [44] A. A. Oughli, F. Conzuelo, M. Winkler, T. Happe, W. Lubitz, W. Schuhmann, O. Rüdiger, N. Plumeré, *Angew. Chem. Int. Ed.* **2015**, *54*, 12329.
- [45] P. Rodriguez Maciá, A. Dutta, W. Lubitz, W. J. Shaw, O. Rüdiger, *Angew. Chem. Int. Ed.* **2015**, *54*, 12303.
- [46] P. Ceccaldi, M. C. Marques, V. Fourmond, I. C. Pereira, C. Léger, *Chem. Commun.* **2015**, *51*, 14223.
- [47] E. Reisner, J. C. Fontecilla-Camps, F. A. Armstrong, *Chem. Commun.* **2009**, *5*, 550.
- [48] N. Plumeré, O. Rüdiger, A. A. Oughli, R. Williams, J. Vivekananthan, S. Pöller, W. Schuhmann, W. Lubitz, *Nat. Chem.* **2014**, *6*, 822.
- [49] M. A. Alonso-Lomillo, O. Rüdiger, A. Maroto-Valiente, M. Velez, I. Rodríguez-Ramos, F. J. Muñoz, V. M. Fernández, A. L. De Lacey, *Nano Lett.* **2007**, *7*, 1603.
- [50] T. Goris, A. F. Wait, M. Saggu, J. Fritsch, N. Heidary, M. Stein, I. Zebger, F. Lendzian, F. A. Armstrong, B. Friedrich, O. Lenz, *Nat. Chem. Biol.* **2011**, *7*, 310.
- [51] S. R. Tabaei, P. Jönsson, M. Brändén, F. Höök, *J. Struct. Biol.* **2009**, *168*, 200.
- [52] D. Axelrod, D. E. Koppel, J. Schlessinger, E. Elson, W. W. Webb, *Biophys. J.* **1976**, *16*, 1055.